Supporting Information

Fabrication of N-doped carbon-coated MnO/ZnMn$_2$O$_4$ cathode materials for high-capacity aqueous zinc-ion batteries

Tianhao Huang[a1], Mingren Cheng[a1], Yuechao Yuan[a], Ze Chang[a,*], Lingjun Kong[a,b,*], Xian-He Bu[a,c]

a School of Materials Science and Engineering, TKL of Metal and Molecule Based Material Chemistry, Nankai University, Tianjin 300350, China

b Institute of Molecular Plus, Department of Chemistry, School of Science, Tianjin University, Tianjin 300072, China

c State Key Laboratory of Elemento-Organic Chemistry, College of Chemistry, Nankai University, Tianjin 300071, China

[1]These authors contributed equally to this work

*Correspondence: ljkong@tju.edu.cn; changze@nankai.edu.cn

Experimental section

1. Synthesis of MnO_2 nanorods

In general, the MnO_2 nanorods are usually prepared by a facile hydrothermal method. Briefly, 0.7013 g $KMnO_4$ was dissolved into 70 mL of deionized (DI) water and then 3.3 mL of concentrated HCl was added to the above solution. After continuous vigorous stirring for 10 min at room temperature, the final solution was transferred into a 100 mL Teflon-lined stainless steel autoclave, which was maintained at 140 °C for 16 h. After cooling to room temperature, the brown MnO_2 precipitate was obtained by centrifugation and washed with DI water and ethanol for three times, respectively. Then, the sample was dried at 60 °C for 12 h.

2. Synthesis of unmodified MnO_x

Unmodified MnO_x was obtained by annealing the MnO_2 prepared by the above method at 700 °C for 4 h under argon atmosphere at a heating rate of 2 °C min^{-1}. The X-ray diffraction (XRD) pattern of the bulk sample consist well with the simulated MnO pattern (PDF No. 00-9864).

3. Synthesis of N-C

The acquisition method ZIF-8 is as follows: a CH_3OH solution (30 mL) of $Zn(NO_3)_2 \cdot 6H_2O$ (0.2974 g), 2-methylimidazole (0.657 g) and PVP (0.375 g) was stirred for 1.5 h at room temperature and the white ZIF-8 precipitate was collected by centrifugation with CH_3OH washing and then dried at 60 °C for 12 h. The XRD pattern of it consist well with the simulated ZIF-8 pattern (Figure S1). The pure N-C was obtained by annealing ZIF-8 precursor under the same conditions as previously described in part 2. As shown in the XRD pattern of N-C, the broad peak at about 23° (2θ) is the characteristic of carbon (002) peak which shows a typical graphite carbon material.

4. Synthesis of MZM@N-C composite

In a typical procedure, a CH_3OH solution (20 mL) of $Zn(NO_3)_2 \cdot 6H_2O$ (0.2974 g) and MnO_2 (0.043 g) is vigorous stirred at room temperature for 1 h. Then a CH_3OH solution (10 mL) of 2-methylimidazole (0.657 g) and PVP (0.375 g) was quickly poured

into the solution. The resultant mixed solution was stirred for 1.5 h at room temperature and the brown MnO_2@ZIF-8 precipitate was collected by centrifugation with CH_3OH washing and then dried at 60 °C for 12 h. Finally, the MZM@N-C nanorods were obtained by annealing the MnO_2@ZIF-8 precursor at 700 °C for 4 h under argon atmosphere at a heating rate of 2 °C min^{-1}.

5. Physical characterizations

The crystal structure of the as-prepared samples was characterized by X-ray diffraction (XRD, Rigaku MiniFlex600, Cu Kα radiation). The morphological structures were observed by scanning electron microscope (SEM, FEI Nanosem 430; Hitachi S-4800), energy dispersive spectroscopy (EDS) mapping, and a high-resolution transmission electron microscope (HRTEM, FEI Tecnai, model G2F-20 field emission TEM). The X-ray photoelectron spectroscopy (XPS) data were recorded on ESCALAB 250Xi X-ray photoelectron spectrometer (Thermo Scientific). The C 1s peak (BE = 284.8 eV) was used as the reference line to accurately determine the positions of other spectral lines. The fine structure of the photoelectron lines was treated using XPSPEAK software. Raman spectrum was collected on RTS-HiR-AM Raman spectrometer (TEO) with laser excitation at 532 nm wavelength. Thermogravimetric analysis (TGA) was performed under an air atmosphere with a heating rate of 10 °C min^{-1} on a Thermo Plus EVO 2 (TG 8121). The N_2 adsorption-desorption isotherms were measured at 77 K by a Micromeritics Tristar II. The specific surface areas of the materials were calculated using the Brunauer-Emmett-Teller method. Pore size distribution of the samples were determined using BJH method.

6. Electrochemical Measurements

For the electrochemical evaluation, the batteries were assembled using the MZM@N-C as the cathode, glass fiber as the separator, and Zn foil as the anode in CR2032 coin cells. The cathode electrode was prepared by mixing MZM@N-C product, Ketjen black, and polyvinylidene fluoride (PVDF) at a weight ratio of 7:1.5:1.5 in N-methyl pyrrolidone solvent. Then, the slurry was pasted on a Ti foil followed by drying under vacuum at 80 °C for 12 h. The electrodes were punched out with diameters of 12 mm and mass loading of 0.9-1.1 mg cm^{-2}. The aqueous electrolyte was 2.0 M

ZnSO$_4$ with 0.2 M MnSO$_4$ in water. The galvanostatic charge/discharge measurements were performed on a LAND CT2001C tester at different current densities with a cut-off voltage window of 0.9-1.8 V. The current density and specific capacity were based on the mass of MZM@N-C in each electrode. Cyclic voltammetry (CV) tests were carried out using a Prinseton VersaSTAT 4 electrochemical workstation (AMETEK) at various scan rates within the potential window of 0.9-1.8 V. Electrochemical impedance spectroscopy (EIS) test was also performed using a Prinseton VersaSTAT 4 electrochemical workstation (AMETEK) with an AC amplitude of 5 mV over the frequency ranging from 100 kHz to 10 mHz.
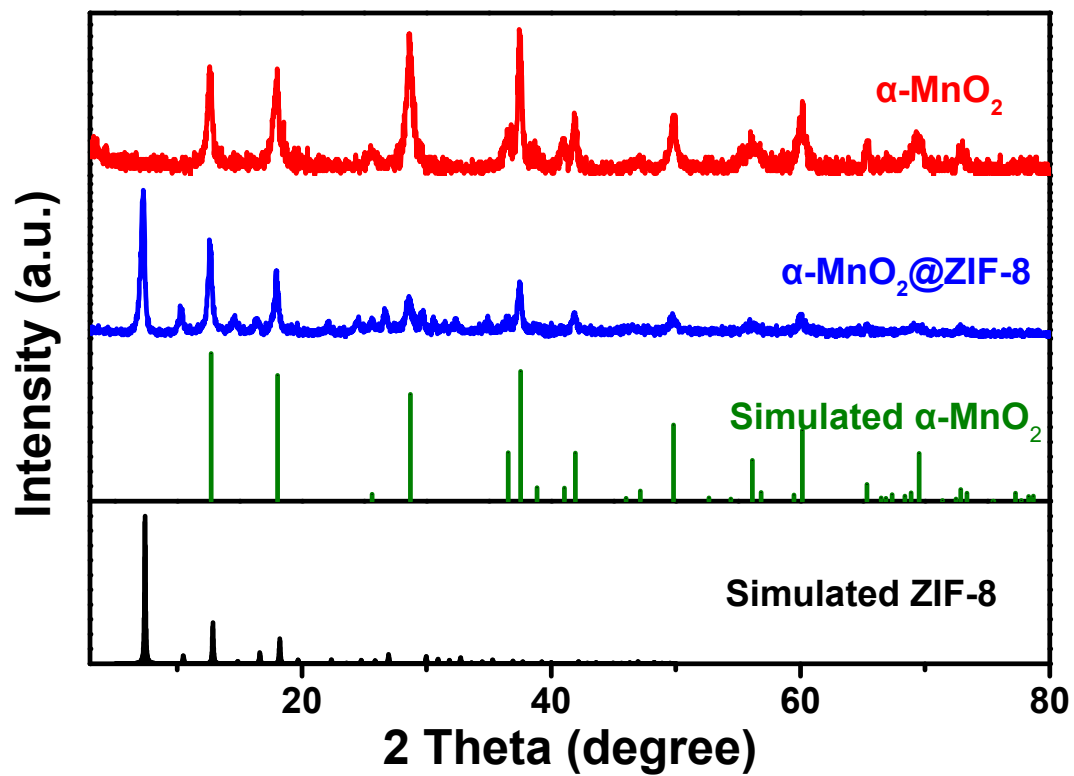
Figures

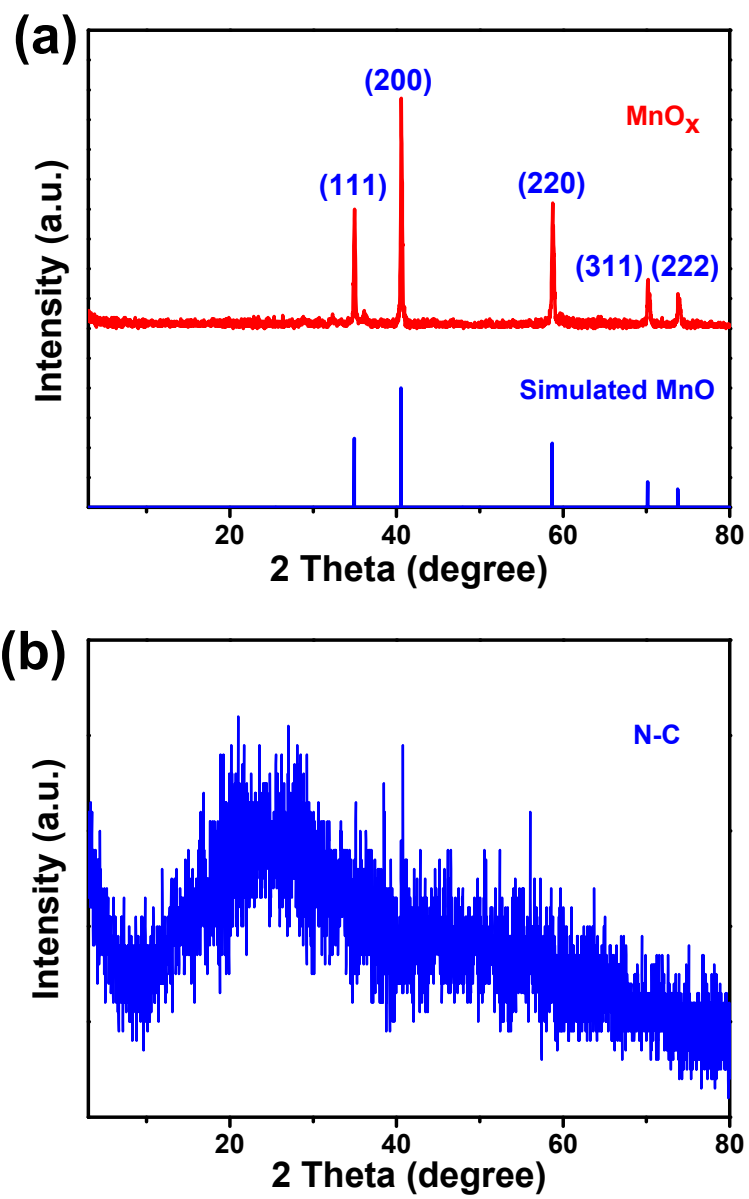

Figure S1. XRD patterns of MnO_2 and $MnO_2@ZIF$-8.

Figure S2. XRD patterns of unmodified MnO_x and N-C.
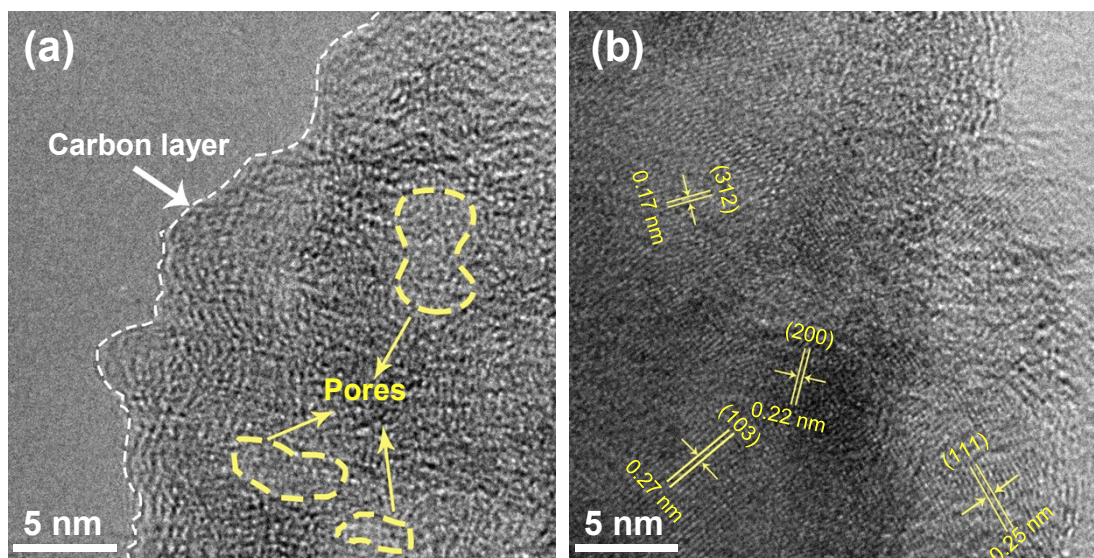
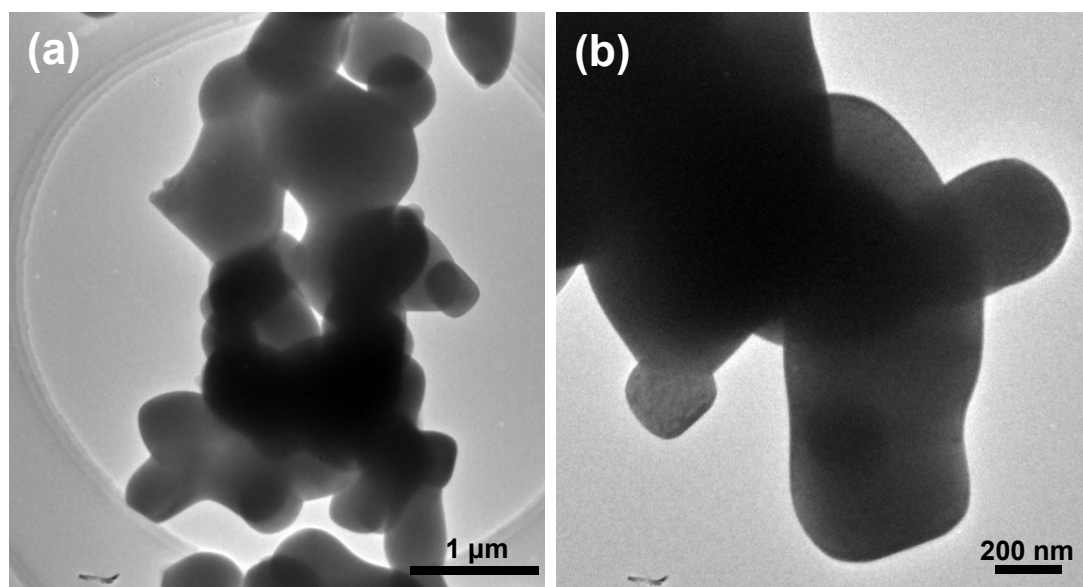**Figure S3.** TEM images of MZM@N-C composite.

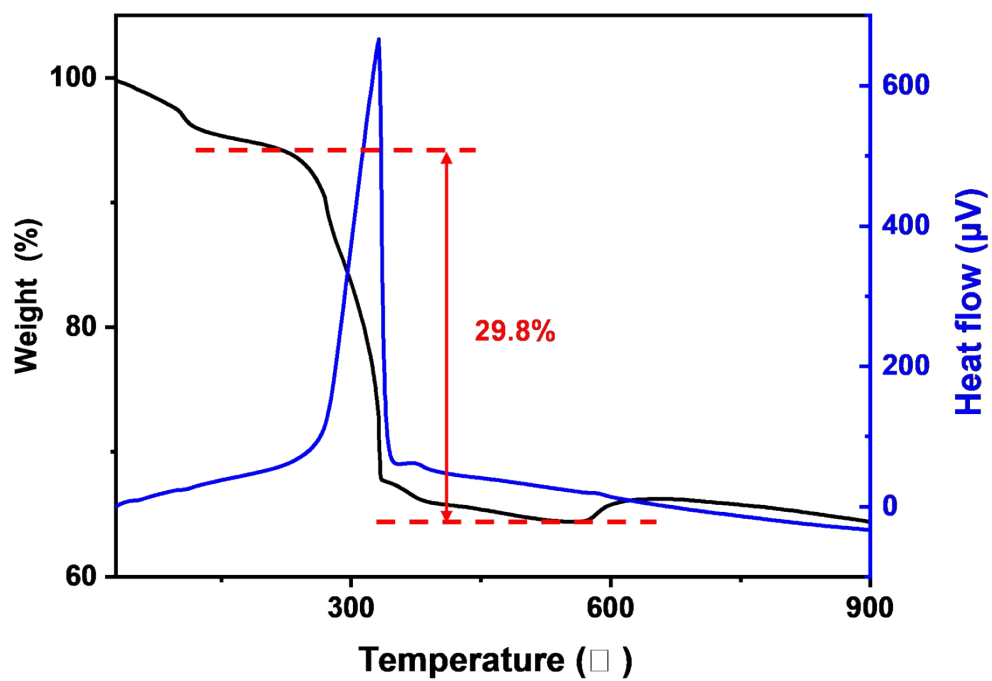**Figure S4.** TEM images of the MnO$_x$.

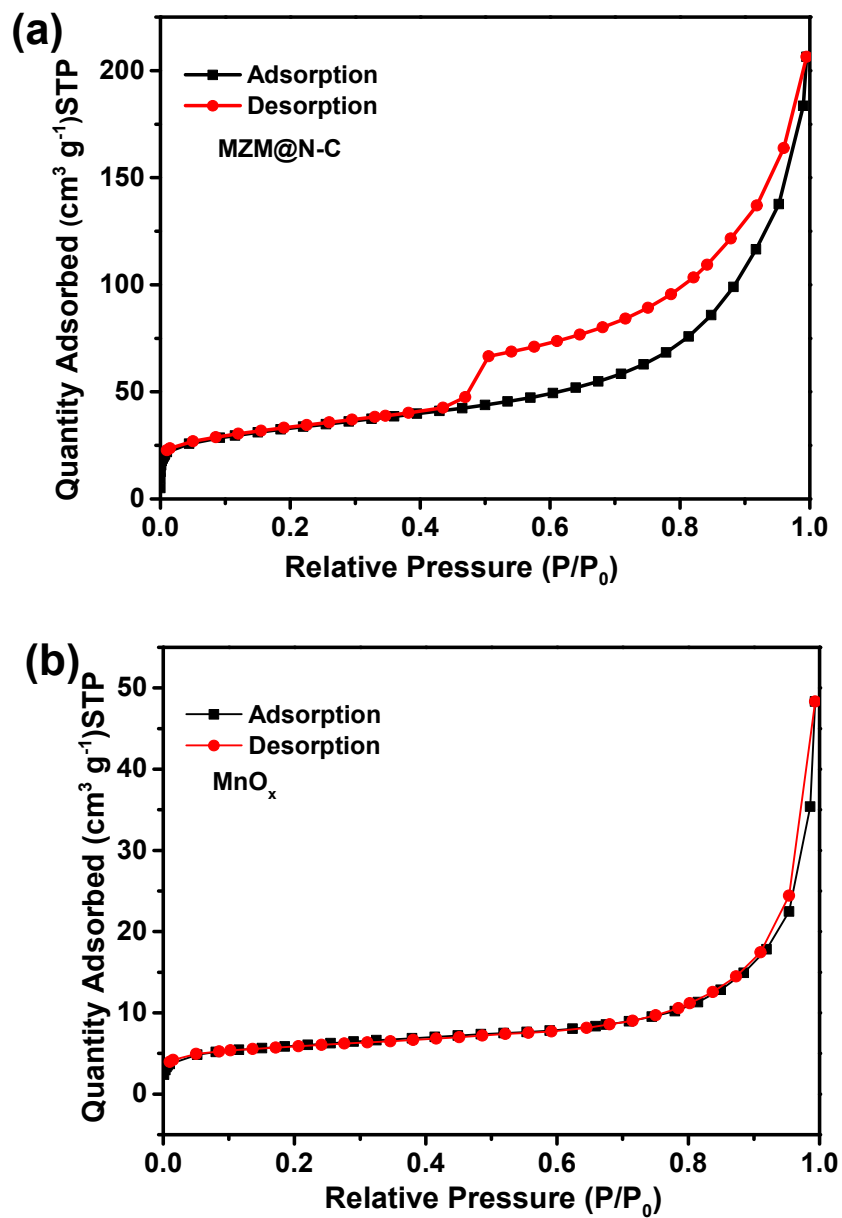**Figure S5.** TGA curve of the MZM@N-C composite.

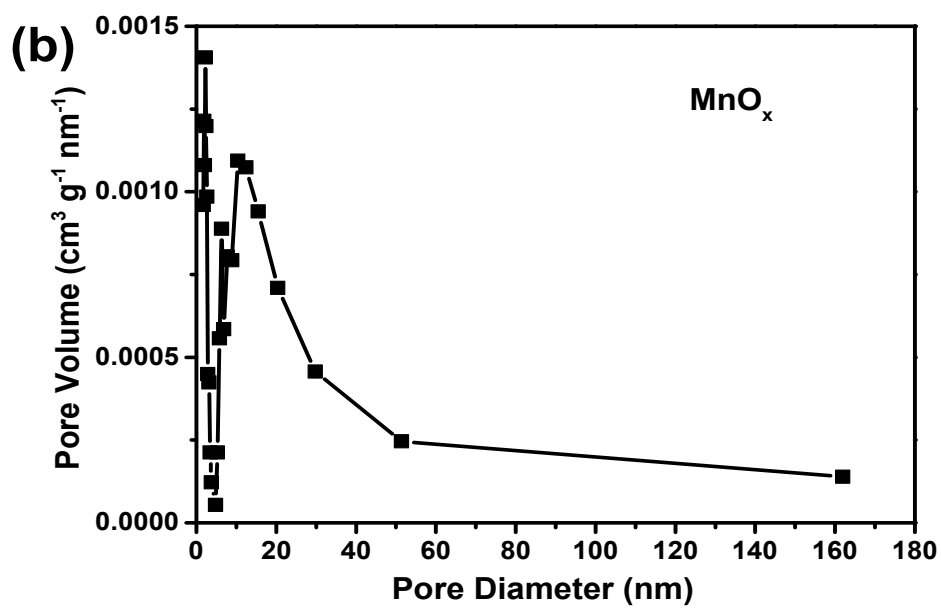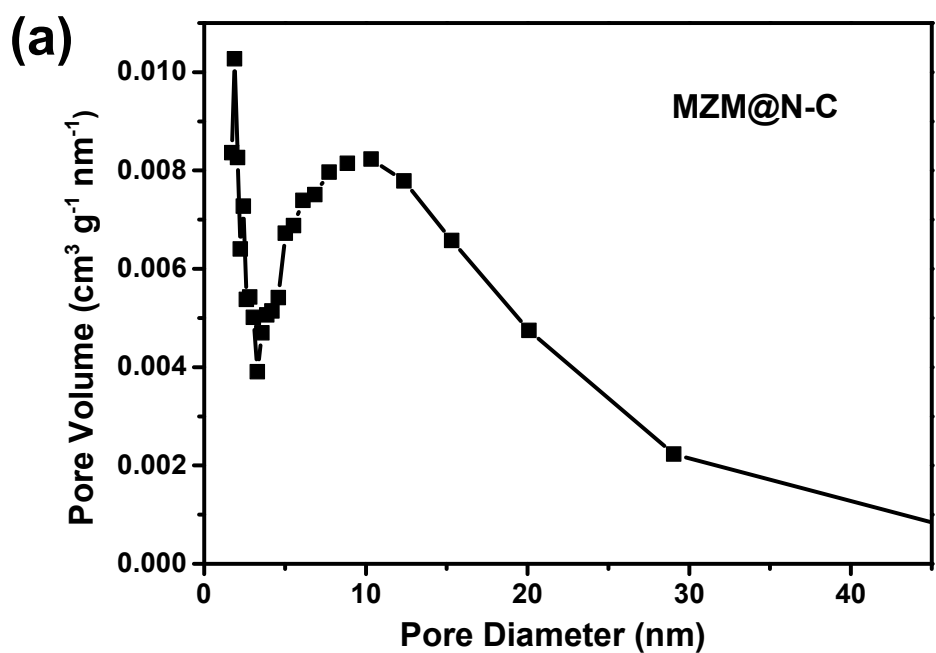**Figure S6.** N_2 adsorption-desorption isotherms of a) MZM@N-C composite and b) MnO_x.

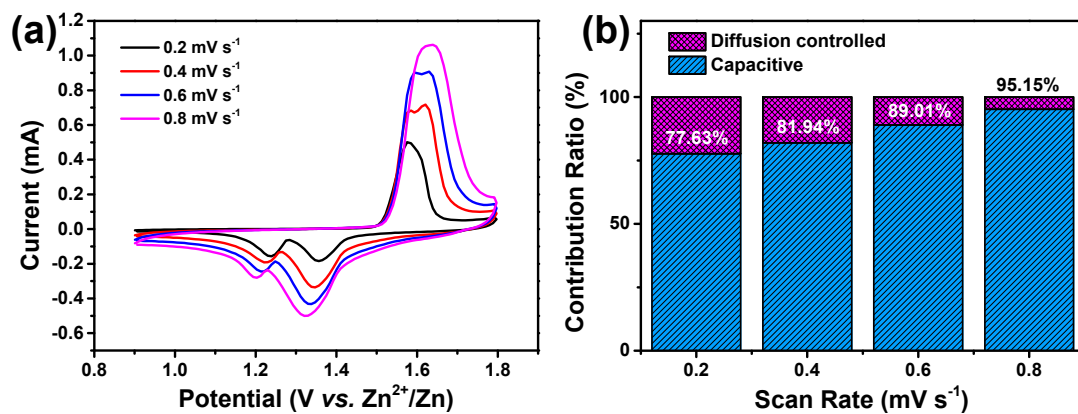**Figure S7.** The pore size distribution of a) MZM@N-C composite and b) MnO_x.

Figure S8. a) CV curves and b) capacity contribution ratios of the MnO_x.

Table S1 Performance comparison of MZM@N-C cathode with other manganese-based cathodes.

Electrode	Specific capacity	Capacity/cycles/current density	Ref.
N-doped MnO_2	183 mAh g^{-1} at 500 mA g^{-1}	103 mAh g^{-1}/1000/5000 mA g^{-1}	1
$ZnMn_2O_4$	223 mAh g^{-1} at 100 mA g^{-1}	137 mAh g^{-1}/1500/2000 mA g^{-1}	2
α-Mn_2O_3	228 mAh g^{-1} at 100 mA g^{-1}	116 mAh g^{-1}/2000/2000 mA g^{-1}	3
ZnO-MnO@C	212 mAh g^{-1} at 100 mA g^{-1}	82.7 mAh g^{-1}/2000/3000 mA g^{-1}	4
MnO	269 mAh g^{-1} at 100 mA g^{-1}	114.6 mAh g^{-1}/300/500 mA g^{-1}	5
δ-MnO_2	278 mAh g^{-1} at 1 C	106.5 mAh g^{-1}/10000/20 C	6
MnO_2/MnO@C	160 mAh g^{-1} at 100 mA g^{-1}	165 mAh g^{-1}/200/500 mA g^{-1}	7
$K_{0.27}MnO_2$·$0.54H_2O$	260 mAh g^{-1} at C/3	84 mAh g^{-1}/1000/10 C	8
MnO@N-C	305 mAh g^{-1} at 500 mA g^{-1}	195 mAh g^{-1}/1600/1000 mA g^{-1}	9
MZM@N-C	**365.5 mAh g^{-1} at 200 mA g^{-1}**	**205 mAh g^{-1}/300/500 mA g^{-1}**	**This work**

Table S2. The physical meanings of the items in the equations.

Items	Physical meaning	Items	Physical meaning
k_1v	current contributions from surface capacitive effects	$k_2v^{1/2}$	current contributions from diffusion-controlled insertion
R	gas constant	T	absolute temperature
A	electrode surface area	n	number of electrons per molecule during oxidation
F	Faraday constant	C	concentration of zinc ion
$σ$	Warburg factor	R_o	ohmic resistance
$R1$	diffusion resistance	Rct	interface faradic charge-transfer resistance
Zw	Warburg impedance	a	tunable parameter
b	tunable parameter		

Table S3. The σ values of MZM@N-C, MnO_x, and N-C before and after cycles.

Samples	σ (before cycles)	σ (after cycles)
MZM@N-C	53.6	38.4
MnO_x	99.8	115.7
N-C	27.1	56.6

References:

1   Y.A. Zhang, Y.P. Liu, Z.H. Liu, X.G. Wu, Y.X. Wen, H.D. Chen, X. Ni, G.H. Liu, J.J. Huang, S.L. Peng, *Journal of Energy Chemistry,* 2022, **64**, 23-32.

2   W.D. Qiu, H.B. Xiao, H.J. Feng, Z.C. Lin, H. Gao, W.T. He, X.H. Lu, *Chemical Engineering Journal,* 2021, **422**, 129890.

3   Y. Ma, Y.J. Ma, T. Diemant, K.C. Cao, X. Liu, U. Kaiser, R.J. Behm, A. Varzi, S. Passerini, *Advanced Energy Materials,* 2021, **11**, 2100962.

4   S. Islam, M.H. Alfaruqi, D.Y. Putro, S. Park, S. Kim, S. Lee, M.S. Ahmed, V. Mathew, Y.K. Sun, J.Y. Hwang, J. Kim, *Advanced Science,* 2021, **8**, 2002636.

5   W.J. Li, X. Gao, Z.Y. Chen, R.T. Guo, G.Q. Zou, H.S. Hou, W.T. Deng, X.B. Ji, J. Zhao, *Chemical Engineering Journal,* 2020, **402**, 125509.

6   D.H. Wang, L.F. Wang, G.J. Liang, H.F. Li, Z.X. Liu, Z.J. Tang, J.B. Liang, C.Y. Zhi, *Acs Nano,* 2019, **13**, 10643-10652.

7   W.W. Jiang, H.T. Shi, X.J. Xu, J.D. Shen, Z.W. Xu, R.Z. Hu, *Energy & Environmental Materials,* 2020, **4**, 603-610.

8   L. Liu, Y.C. Wu, L. Huang, K. Liu, B. Duployer, P. Rozier, P.L. Taberna, P. Simon, *Advanced Energy Materials,* 2021, **11**, 2101287.

9   Y.Q. Fu, Q.L. Wei, G.X. Zhang, X.M. Wang, J.H. Zhang, Y.F. Hu, D.N. Wang, L. Zuin, T. Zhou, Y.C. Wu, S.H. Sun, *Advanced Energy Materials,* 2018, **8**, 1801445.